# Atmospheric Effect on Spectral Signature—Measurements and Corrections

YORAM J. KAUFMAN

*Abstract*—**In order to improve the quality of remote-sensing data there is a need to estimate the atmospheric effect from the image itself. This can be done by recognition of some surface features with known reflection properties. For this purpose, measurements of the atmospheric effect on the spectral signature of surface cover were conducted during hazy conditions over the Chesapeake Bay and its eastern shore. In the experiment the upward radiance was measured by an airborne scanning radiometer in nine spectral bands between 465 and 773 nm, above and below the haze layer. Simultaneous measurements of the aerosol optical thickness and its vertical distribution were conducted. The results of the measurements are used here to study the spectral dependence of the atmospheric effect on remote sensing of water bodies and vegetated fields (forest, corn field, and pasture), and to verify theoretical predictions. It is suggested that the radiances over dark areas (e.g., water in the near IR and forest in the visible) can be used to derive the aerosol optical thickness as is done over oceans with the CZCS satellite images. Combined with climatological information, the derived optical thickness can be used to perform corrections of the atmospheric effect. Examples of the derivation of the aerosol optical thickness and correction of the upward radiances are given.**

## I. Introduction

ATMOSPHERIC aerosol and molecules scatter and absorb solar radiation, thus affecting the downward and upward radiance detected above the earth's atmosphere. The atmospheric scattering and absorption depend substantially on the wavelength of the radiation. Scattering is usually much stronger for short wavelengths than for long wavelengths. The magnitude of molecular scattering varies as $\lambda^{-4}$ [1], where $\lambda$ is the wavelength of the radiation. The magnitude of the aerosol scattering varies as $\lambda^{1}$ to $\lambda^{-3}$. The scattering coefficient of the Saharan dust is usually wavelength independent [2] and [3] while industrial pollution that extends over the Eastern United States generates an aerosol with a $\lambda^{-2}$ dependent scattering [4].

Due to its strong wavelength dependence, atmospheric scattering affects the classification of surface features [5] and the remote sensing of the vegetation index [6] and [7]. But the same wavelength dependence of the atmospheric effect may provide a measure for its determination. The atmospheric effect on remote sensing was discussed in the literature from a theoretical point of view [6], [8], and [9]. In order to measure the atmospheric effect and its wavelength dependence, a field experiment was conducted [10]. In the experiment the atmospheric effect on the upward radiance was measured by an airborne scanning radiometer. The aircraft flew close to the ground (300 m) and measured the radiance entering the atmosphere from below (this radiance is affected by the aerosol in the lowest 300 m), and also flew at 3800 m, above the haze, where the measurements of upward radiance were affected by the atmosphere [10]. While the previous paper [10] emphasized the spatial degradation of the contrast due to the atmospheric effect, the present paper studies the spectral atmospheric effect on remote sensing of water bodies and vegetated fields. Suggestions for atmospheric corrections also are given and tested.

Manuscript received September 3, 1986; revised June 22, 1987.

The author is with the NASA/Goddard Space Flight Center, Greenbelt, MD 20771.

IEEE Log Number 8716475.

## II. Experimental

A detailed description of the experiment was given elsewhere [10]; therefore, only a short review of the setup is given here. The spectral characteristics of the system are discussed in detail. The experiment included three measuring systems:

### A. Airborne Scanning Radiometer

The Ocean Color Scanner (OCS) was mounted on the NASA Skyvan aircraft to collect digital images of the upward radiance. The radiance was detected at nine narrow spectral channels in the visible and near IR parts of the spectrum (see Table I). The radiometer scanned the upward radiance from $-45°$ to $+45°$ from the nadir. The aircraft was flown at two altitudes: 300 m (under most of the aerosol layer) and 3800 m (above most of the haze). The OCS was calibrated before the flight using an integrating sphere calibrator and the calibration was verified by comparing the low flight radiances with ground measurements of the upward radiance [10].

### B. Aerosol Sampler

During the OCS flights, profiles of the aerosol scattering coefficient were measured by an airborne nephelometer developed at the University of Wisconsin. The air temperature and dew point were also measured as a function of time and the aircraft location and altitude.

### C. Ground Measurements

The wavelength dependence of the aerosol optical thickness was measured from the ground at four sites. The scattering coefficient was also measured at the ground at

TABLE I
SPECTRAL CHANNELS ON THE OCS RADIOMETER

| channel | wavelength (nm) | width (nm) |
|---|---|---|
| 1 | 465 | 28 |
| 2 | 495 | 28 |
| 3 | 524 | 29 |
| 4 | 556 | 30 |
| 5 | 587 | 30 |
| 6 | 619 | 32 |
| 7 | 652 | 29 |
| 8 | 682 | 30 |
| 9 | 773 | 51 |

the OCS flying site. The optical thickness was measured by four sunphotometers; two had eight spectral bands from 440 to 1030 nm, and two had four bands from 370 to 945 nm.

The data presented were collected on 9/10/82 over the eastern shore of Chesapeake Bay, around 1 P.M. Eastern Standard Time. On this day a dense haze developed during a few days of meteorological stagnation conditions over the Eastern United States [10].

## III. ATMOSPHERIC EFFECT

The atmospheric effect is caused by molecular and aerosol scattering and absorption of solar radiation. It can be described as composed of the following components (see Fig. 1):

*1) Effect on Downward Radiation:* The downward solar radiation is attenuated by absorption and backscattering in the atmosphere, and it is diffused from the direct beam by forward scattering. The diffusion increases the angular distribution of the radiation and, therefore, causes the radiation to interact with the surface in a wide range of directions (instead of the direction of the solar beam). As a result, the reflection coefficient of the surface that corresponds to this radiation will not be equal to the reflection coefficient of the direct solar beam [8].

*2) Effect on Upward Radiation:* Radiation reflected from the ground is attenuated further by atmospheric absorption and backscattering. Scattering also causes diffusion of the radiation, thus introducing into the field of view photons that were reflected from the area out of the field of view [11].

*3) Atmospheric Path Radiance:* Light is scattered in the atmosphere from the direct solar beam into the field of view, without being reflected by the surface. This component brightens the image. Its effect is particularly significant for dark surfaces.

For an empty atmosphere (no atmospheric effect) the upward radiance ($L_e$) detected by a satellite over a uniform Lambertian surface of reflectance $\rho$ would be

$$L_e = F_0 \mu_0 \rho \tag{1}$$

where $F_0$ is the extraterrestrial solar flux, and $\mu_0$ is cosine of the solar zenith angle. Once the atmospheric effect is included, the relation between the upward radiance and the surface reflectance becomes [12], [13]

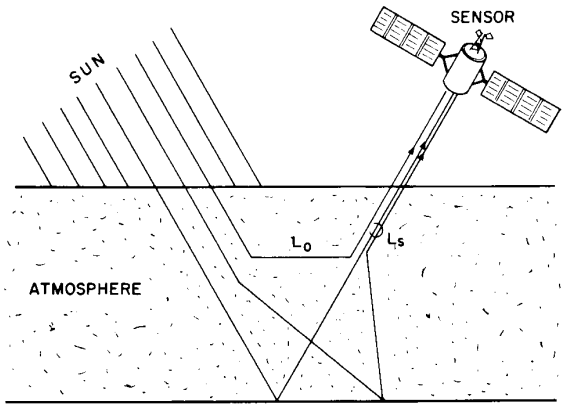


Fig. 1. Schematic diagram of the atmospheric effect on remote sensing.

$$L(\theta, \psi, \theta_0) = L_0(\theta, \psi, \theta_0) + \rho F_D(\theta_0) T(\theta) / [\pi(1 - s\rho)] \tag{2}$$

where $\theta$ and $\psi$ are the zenith and azimuthal angles of the direction of propagation of the light; $F_D$ is the total downward flux of light at the ground for surface reflectance $\rho = 0$ (it represents the atmospheric effect on the downward radiation); $T$ is a transmission function from the ground to the top of the atmosphere for the radiance (it represents the atmospheric effect of the upward radiation); and $s$ is the reflectance of the atmosphere for isotropic light entering the base of the atmosphere. The first term on the right-hand side of (2) is just the radiance of the atmosphere for a nonreflecting ground ($\rho = 0$). This term is the path radiance $L_0$ discussed before.

In Fig. 2 a particular example is given of the spectral surface reflectance (Deering, private communication) for a typical vegetation (assumed to be Lambertian), and the corresponding calculated upward radiance [13] above the atmosphere, normalized by the incident solar flux ($F_0 \mu_0$) to reflectance units. Note that this normalized radiance is equal to the surface hemispherical reflectance for no atmospheric effect. Once the atmospheric effect is present, the normalized radiance is equal to the apparent surface reflectance as seen from space. For the visible part of the spectrum ($\lambda < 750$ nm), due to the low surface reflectance, the atmospheric effect is dominated by the path radiance, and the upward radiance above the atmosphere is substantially higher than at the bottom of the atmosphere. This effect increases with a decrease of the wavelength of the radiation. In the near IR ($\lambda > 750$ nm) vegetation has a high surface reflectance, and as a result the atmospheric attenuation is dominant [13]. In the example of Fig. 2 a relatively clear atmospheric model was used, with aerosol optical thickness

$$\tau_a = 0.25(550/\lambda) \tag{3}$$

where $\lambda$ is the wavelength (nm). The aerosol model chosen has low absorption ($\omega_0 = 0.96$ where $\omega_0$ is the ratio

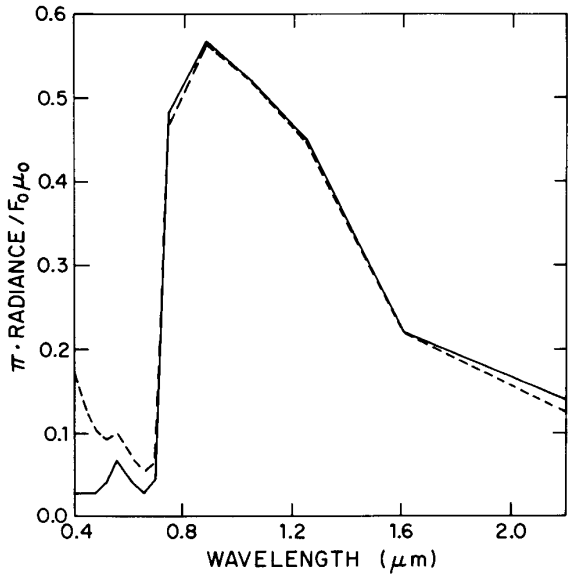


Fig. 2. Surface reflectance (——) and the corresponding upward radiance (- - - -) above the atmosphere for a typical vegetation. The radiance is normalized by $F_0$, the incident solar flux, and by $\mu_0$, the cosine of the solar zenith angle.

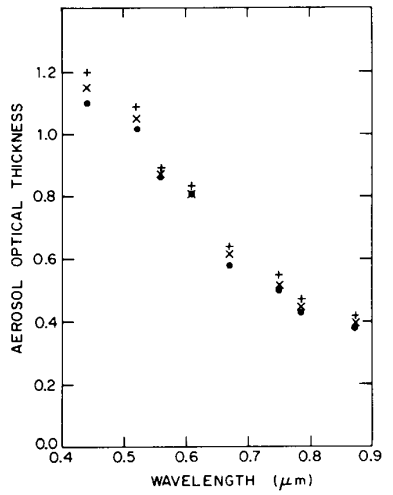


Fig. 3. The measured aerosol optical thickness over the eastern shore of Chesapeake Bay, as a function of the radiation wavelength (•) for 12EST, (+) for 13EST, and (×) for 14 EST.

of aerosol scattering to aerosol scattering + absorption coefficients). For higher aerosol absorption the atmospheric attenuation in the near IR would be substantially stronger, and the brightening (for short wavelengths) somewhat weaker [13].

## IV. Measurements

During the experiment the atmosphere was very hazy. The haze was around four times denser than the global average. These conditions are rather common during the summer months in the Eastern United States [4], [14]. The measured aerosol optical thickness is shown in Fig. 3. The aerosol optical thickness decreased sharply with wavelength. The different measurements in Fig. 3 show that the optical thickness varied by only 5–10 percent during the OCS flight.

The upward radiances detected over: a forest, a corn field, a pasture field, the Chesapeake Bay, and a small lake are shown in Figs. 4–8, respectively. The radiances are normalized to reflectance units. The radiances detected during the low and the high OCS flights are shown. The simulated upward radiance at the surface, described below, is also plotted. In these figures six OCS channels are used (channels 1, 2, 4, 6, 8, and 9 in Table I). The plotted radiances are averages of the measured radiances over the given sites (forest, corn field, etc.). In each average between 20 to 200 data points were used.

There are differences between the spatial resolution of the radiances derived from the low and the high flight data as well as the directions from which the radiances were collected. These differences affect the data quality. The low flight is about 10 times closer to the ground than the high flight. Therefore, for the same area the low flight radiances were averaged over 100 times as many pixels as the high flight radiances. Although much care was given to identify the same areas in the low and high flights for measuring the atmospheric effect, the presence of the aircraft roll and the different sampling density generated some differences between the sampled areas in the two flights. There also is a difference in the solar orientation between the low and the high flights, which were taken about 1 h apart. Due to this time difference, the surface reflectance that affected the radiance in the two flights might be somewhat different. This effect is important mainly for vegetation in the near IR, which, due to its high reflectivity, has a pronounced effect on the radiance. In Figs. 4–8 the path radiance is dominant for the dark vegetation in the visible part of the spectrum, and is similar to the computations of Fig. 2. For $\lambda = 780$ nm, due to the bright vegetation, the atmospheric effect results usually in decreasing the upward radiance (Figs. 4–6). The magnitude and the direction of the atmospheric effect on a bright surface depends on the balance between atmospheric scattering and absorption [13]. For the dark water in the near IR, the atmospheric effect is again of brightening (the radiance detected in the high flight is much larger than the radiance detected in the low flight—Fig. 7). In the case of the small lake surrounded by vegetation (Fig. 8), the high reflectivity of the vegetation in the near IR (773 nm) causes the radiance above the lake to be brighter in the near IR than in the visible due to the adjacency effect [11], [15], [16], and [17]. In this case, when the detector observes the lake, the radiance reflected from the bright vegetation surrounding the lake is scattered by the atmosphere into the field of view of the detector.

## V. Simulations

In order to test our theoretical knowledge of the atmospheric effect the upward radiance in the high flight is

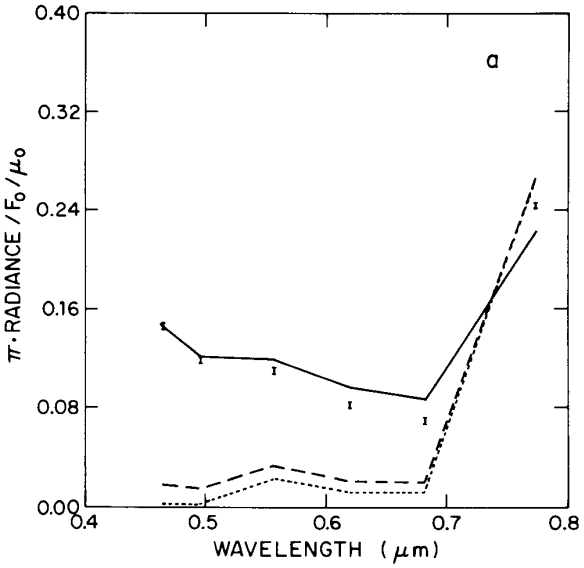


(a)

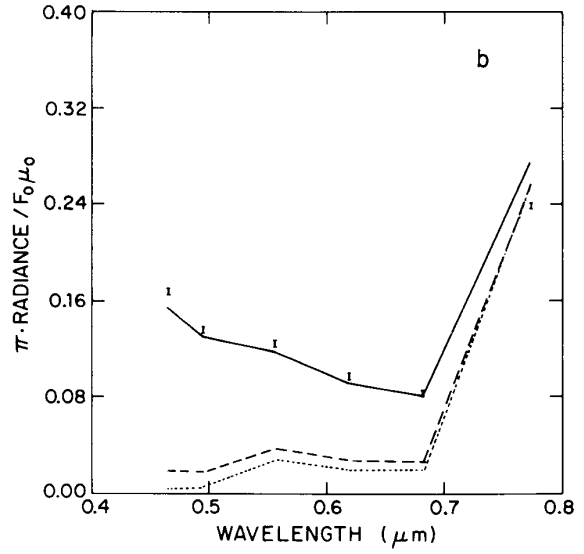


(b)

Fig. 4. The upward radiance measured by the Ocean Color Scanner detector at 300 m (---) and at 3800 m (———). The radiance at 300 m is corrected for the lowest 300 m of the atmosphere (·····). The bars represent the theoretical simulation for the upward radiance using the optical thickness measured from the ground. (a) is forest nadir observation. (b) is forest $\theta = 28°$.

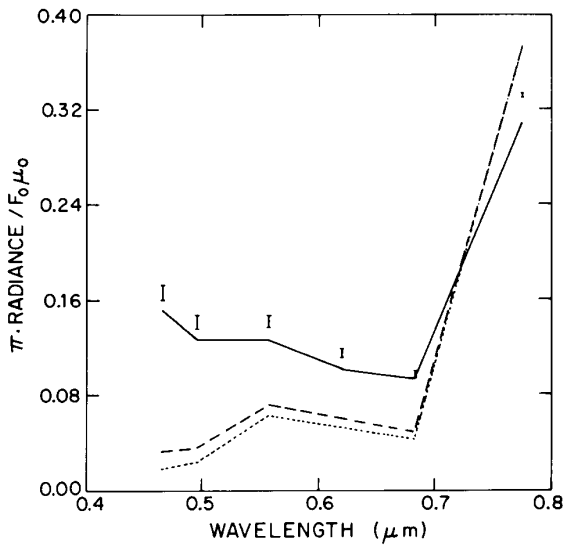


Fig. 5. Same as in Fig. 4 but for corn $\theta = 24°$, $\psi = 120°$.

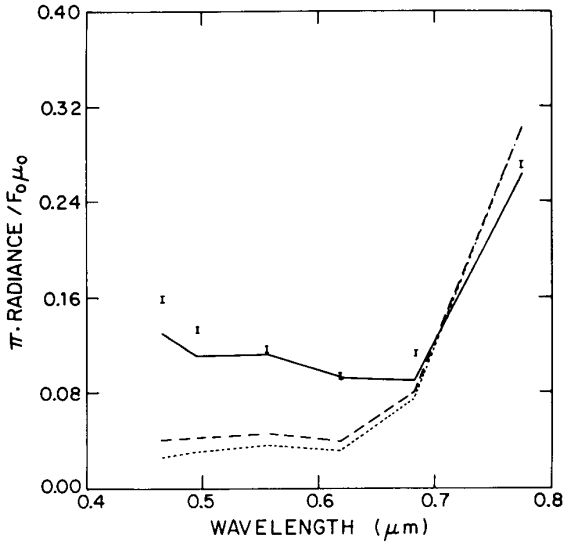


Fig. 6. Same as in Fig. 4 but for pasture $\theta = 4°$, $\psi = 120°$.

simulated by radiative transfer conputations and compared with measurements. The input data to the simulation are the radiances in the low flight (transformed into the surface reflectance) and the aerosol spectral optical thicknesses. The computations are performed by the Dave and Gazdag [18] radiative-transfer model. This model is used to compute the upward and downward radiance in a plane-parallel atmosphere with a uniform Lambertian surface. The version of the model used here neglects polarization. Since this model requires a Lambertian surface (that should represent a non-Lambertian vegetation), a different (Lambertian) value of the surface reflectance was used for each observation direction. The surface reflectance was obtained from the low flight radiances measured in this particular direction. This method was tested in a theoretical study by Lee and Kaufman [8] and found applicable for remote sensing of the surface reflectance. That study showed that the error in the surface reflectance ($\rho$) introduced due to the Lambertian assumption (for observation zenith angle $\theta < 45°$) is less than $\Delta\rho = 0.005$.

In order to convert the low flight radiance into surface reflectivity, the radiance was corrected for the atmospheric effect in the lowest 300 m of the atmosphere (under the low flight). The aerosol optical thickness for the

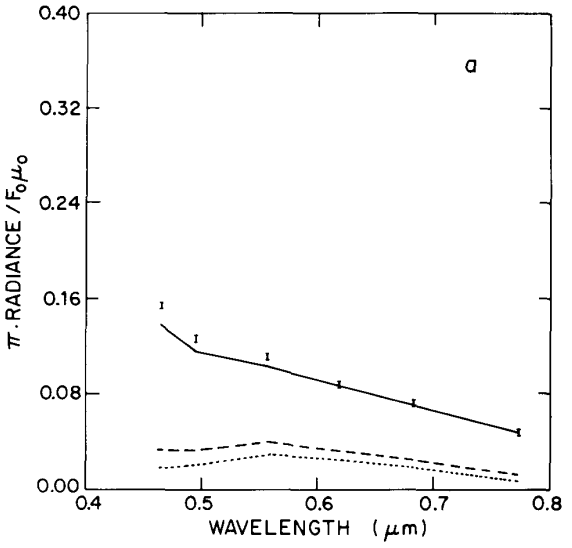


(a)

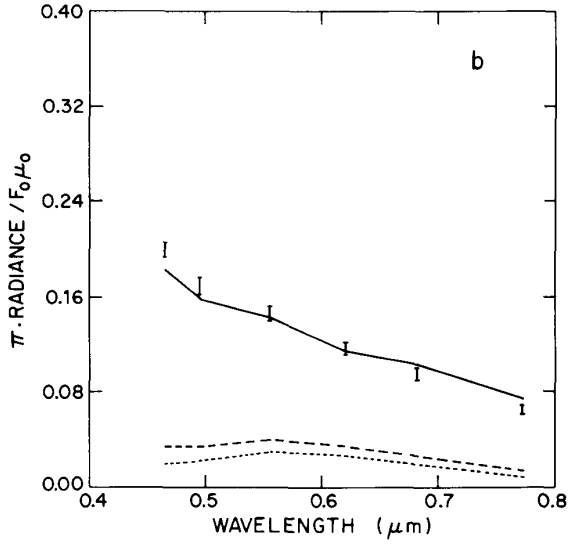


(b)

Fig. 7. Same as in Fig. 4 but for water over the Chesapeake Bay, (a)-nadir observation, (b)-$\theta = 38°$, $\psi = 60°$.

300-m aerosol layer was estimated from the atmospheric scattering profile [10] to be 14 percent of the entire aerosol optical thickness. The radiances at the ground, derived in this way, are also plotted in Figs. 4–8. The surface reflectance was derived from the corrected radiances by dividing them by the solar flux reaching the earth's surface. This flux was computed theoretically by the Dave and Gazdag [18] model (for $\lambda = 773$ nm the computed downward flux was compared successfully with its measurements from the surface [10]). The simulation as well as all the computations in this paper are for an aerosol with refractive index $n = 1.43\text{-}0.0035i$ and a power-law size distribution [19] with a power that corresponds to the average aerosol characteristics in the Washington, DC

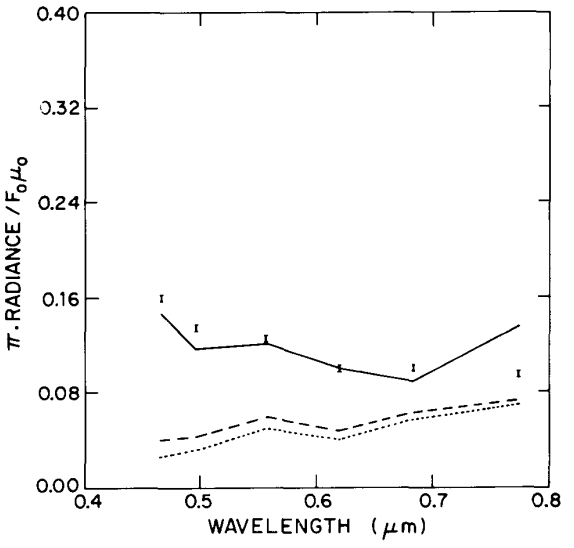


Fig. 8. Same as in Fig. 4 but for a lake on a vegetated background, $\theta = 10°$, $\psi = 120°$.

area during the summer [4]

$$dN/d \ln R = cR^{-3.7}. \tag{4}$$

where $R$ is the particle radius and $dN/d \ln R$ is the logarithmic size distribution.

The simulated radiances as a function of the wavelength are shown in Figs. 4–8. The average of the absolute deviations between the simulated radiance and the measured radiance is 8 percent. In the short wavelengths the simulated radiances are higher than the measured radiances by 3–20 percent. This systematic error can be due to an error in the assumed phase function, error in the measured optical thickness, and some small contribution due to ignoring polarization in the radiative transfer computations. Polarization can affect the radiance through multiple scattering. Since scattered light is affected by polarization mainly in the backscattering direction [20], the polarization effect is introduced mainly through molecular scattering (molecules have a much stronger backscattering than aerosol). As a result, the polarization effect on radiance is more significant for high molecular optical thickness or short wavelengths. Computations with a radiative transfer model that includes polarization [21], [8] show that polarization can introduce an error of 4 percent for $\lambda = 450$ nm but less than 1 percent for $\lambda > 600$ nm, due to the decreasing effect of molecular scattering [22]. There also is a random error in the data that is introduced mainly due to differences in the sampling of the surface by the OCS between the low and high flights, and the difference in the solar direction described above. As expected, the theoretical model that assumes a uniform surface reflectance fails to predict the adjacency effect over the lake in the near IR (Fig. 8) due to light reflected from the bright land surrounding the lake [10]. The high flight radiances and the corresponding simulation show the de-

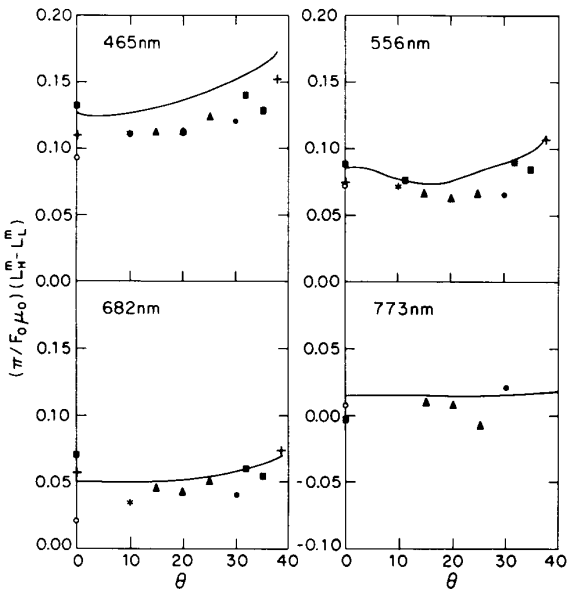


Fig. 9. The difference between the upward radiance at 3800 m ($L_H$) and the upward radiance at 300 m ($L_L$). The symbols represent the experimental points and the solid line the theoretical simulation. The radiance difference is plotted as a function of the observation zenith angle, for all the surface covers given in Figs. 4–8 for each wavelength. (▲)-corn, (•)-pasture, (■)-forest, (+)-water in the bay, and (*)-water in the lake. The radiance difference is normalized to reflectance units.

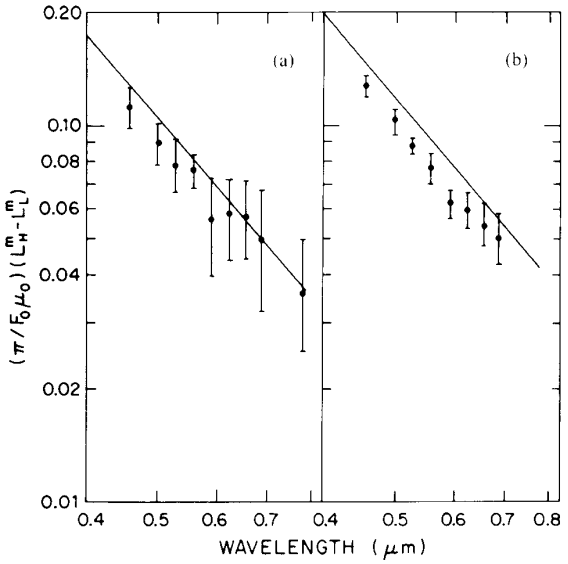


Fig. 10. The radiance difference (defined in Fig. 9), as a function of wavelength. (a) is low observation zenith angles ($\theta < 15°$). (b) is high observation zenith angles ($25° < \theta < 36°$). The bars represent the experimental radiances and their range of variation. The solid line is the theoretical simulation.

pendence of the atmospheric effect on wavelength and on the observation zenith angle.

In Fig. 9 the effect of the observation direction is enhanced by displaying the atmospheric effect measured in all the cases of Figs. 4–8 for each wavelength. The atmospheric effect is calculated here as the difference between the radiance at the high flight and the radiance at the low flight. This difference approximates the path radiance for the visible part of the spectrum, since the surface reflectivity here is much weaker than the atmospheric backscattering. The atmospheric path radiance contributes 50 percent of the upward radiance at the top of the atmosphere for the red part of the spectrum (680 nm) and up to 80 percent in the blue (465 nm). The path radiance (divided by $F_0\mu_0$) increases with the observation zenith angle for zenith angles above 20° due to the longer optical path $-\mu_0^{-1}$ and different value of the scattering-phase function. The noise in the data is due to the different sampling in the low and high flights, and due to variation of the surface reflectance from one surface cover to another. This noise increases with wavelength, due to the increase in the surface reflectance (except water), and decrease in the atmospheric effect. For a wavelength of 773 nm, the vegetation is bright and the difference in radiance represents the combined atmospheric effect of brightening by the path radiance and darkening by absorption and backscattering. The simulated radiance difference is also shown in the figure. It is systematically higher than the measured one by 17 percent for 465 nm, decreasing to 13 percent for 556 nm and 9 percent for 682 nm. The wavelength dependence of the radiance difference is shown in Fig. 10. Here the results for each wavelength from all surface covers are condensed (except for 773 nm over vegetation). The error bars represent the standard variation between the experimental radiances. The theoretical fit is also presented. This simulation shows that radiative transfer computations, with the presently measured and assumed atmospheric and surface characteristics can be used to test methods of atmospheric correction and methods for remote sensing of the atmospheric optical characteristics. The surface-bidirectional reflectance characteristics combined with the difference in the sampling procedure between the low and the high flights, and the time difference between the flights, are the main sources of errors. Uncertainties in the aerosol scatter-phase function also contribute to errors. The error in the aerosol scattering-phase function can be reduced in future experiments by additional measurements of this function (by solar almucantar measurements [23], [24]), and errors in sampling can be reduced by stable and more systematic data collection.

## VI. Remote Sensing of Optical Thickness

The experimental data sets of the low and the high flight radiances and the aerosol optical thicknesses ($\tau_a$) are used here to test methods for the derivation of $\tau_a$ from satellite imagery over land. Such a method was applied to the GOES imagery [25]. A new method for the derivation of $\tau_a$ also will be suggested. The aerosol optical thickness is one of the major parameters needed for atmospheric corrections [17] and if derived for a few wavelengths, can be inverted into the aerosol size distribution [26]. The size distribution can be used to compute the scattering-phase

function that is used in the correction of the atmospheric effect.

The aerosol-optical thickness $\tau_a$ can be derived from radiances detected by satellite platforms (corresponding to the high flight radiances) by using measurements of the surface reflectance performed on the earth's surface or close to it (the low flight). To derive the optical thickness from the radiances detected in the high and low flights, a look-up table was constructed of computed radiances at the high flight $L_H^l$ as a function of $\tau_a$ and the surface reflectance ($\rho$), for the wavelengths used in the experiment. The aerosol model described before was used in the computations. Since the low flight radiances are measured rather than the actual surface reflectance, the surface reflectance ($\rho$) in the look-up table was converted into the low flight radiances ($L_L^l$) by

$$L_L^l = \rho F_D / [\pi(1 - s\rho)] \tag{5}$$

where $F_D$ is the downward flux reaching the surface and computed for each value of $\tau_a$ in the look-up table. With the help of (5) the look-up table $L_H^l(\rho, \tau_a)$ is transformed into $L_H^l(L_L^l, \tau_a)$. For a given measured radiance in the low flight: $L_L^m$ the function $L_H^*(\tau_a)$ is interpolated from $L_H^l(L_L^l, \tau_a)$ for $L_L^l$: $L_L^m$. The aerosol optical thickness $\tau_a$ is interpolated from $L_H^*(\tau_a)$ for the measured radiance in the high flight: $L_H^m$. The derived value of $\tau_a$ corresponds to the difference in the optical thickness between the high and the low flight levels. Note that in this analysis of atmospheric effect the aerosol under the low flight is considered as part of the surface.

In Fig. 11 plots are shown of aerosol optical thickness derived by this procedure from the radiances recorded during the high and low flights. This method of derivation is similar to the method of Fraser *et al.* [25], where the optical thickness was derived from the measured radiances on hazy and clear days.

In order to correct remotely sensed images, for the atmospheric effect, a method is needed to derive the optical thickness from the same image that is corrected. In this case, some assumption on the surface reflectance ($\rho$) has to be made. The method is most useful for dark surfaces, where the error ($\Delta\rho$) in the estimation of the surface reflectance is small, and the radiances detected by the satellite show the greatest dependence on the atmospheric effect. Such a method was applied to images of oceans [27], but not for land. Here the method is applied to the high-flight radiances for the derivation of $\tau_a$ and assuming surface-reflectance values taken from literature [28]. The optical thicknesses derived in these two methods are compared with optical thicknesses measured from the ground (solid lines in Fig. 11). The optical thickness ($\tau_a$) derived from the radiances recorded during the low and the high flights are plotted by (I---I---I) and $\tau_a$ derived using only the high flight radiances by ( ). In this case the low flight radiances were replaced by Kriebel's measurements of vegetation reflectance [28]. Fig. 11(a) and (b) shows the aerosol optical thicknesses derived over the forest (using Kriebel's coniferous forest reflectances). Note that $\tau_a$ derived from the high and low flight data represents the optical-thickness difference between the two flights and not the total vertical values. Therefore, $\tau_a$ derived from the high flight only and $\tau_a$ measured from the ground were scaled to values corresponding to the difference in optical thickness between the two flights. The derived aerosol optical thickness over water is given in Fig. 11(c), over corn in Fig. 11(d), and over pasture in Fig. 11(e). In Fig. 11(d) and (e) Kriebel's pasture reflectivities are used as the surface reflectance in the derivation by the second method. The error bars on the derived optical thickness (Fig. 11) represent the errors due to uncertainty in the OCS scanning direction. A very good agreement was found between the derived optical thicknesses and the measured optical thickness for radiances over water (Fig. 11(c)) and over the forest for off-nadir observation (Fig. 11(a)). The good agreement between the measured and the derived optical thickness over the forest and the water is due to the low reflectivity of these two surfaces. Note that the forest, in the current experiment, does not consist of the same type of trees for which Kriebel's data are given. The method is still useful, since both forests are dense vegetation covers and, therefore, have small reflectances in the visible part of the spectrum (except around 600 nm). Both forests also have a high light-trapping efficiency, thus reducing the reflectance even further.

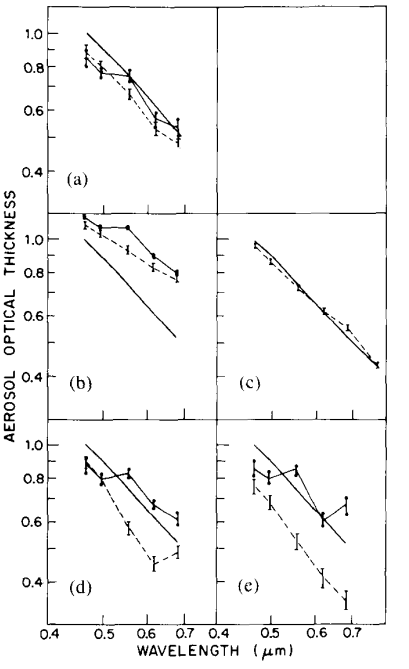


Fig. 11. The aerosol optical thickness measured (solid line), derived from the low and the high flights (I---I), and derived from the high flight and from Kriebel's data (|---|---|). (a) is forest, $\theta = 28°$; (b) is forest, nadir observation; (c) is water, nadir observation; (d) is corn, $\theta = 24°$, $\psi = 120°$; (e) is pasture, $\theta = 30°$, $\psi = 120°$.

Except for water, the near IR radiances were not used to derive the optical thickness due to the high reflectivity

of the vegetation. The optical thickness derived over the forest for nadir view, from the low and the high flights, agreed with the optical thickness derived from the high flight and Kriebel's reflectances, but did not agree with the measured optical thickness. These differences probably result from the introduction of bare soil areas to the radiances used in the high flight. For the off-nadir view this problem did not occur. In Fig. 11(d) and (e), the higher reflectances of the corn and the pasture land, together with sampling problems, introduced high errors in the derived optical thickness in both methods. The good agreement between the optical thickness derived over the forest using Kriebel's reflectances and high flight radiances suggests that dark surfaces over the land, as forest in the visible part of the spectrum and water in the near IR, can be used to derive the aerosol optical thickness for atmospheric corrections. The optical thickness can be derived for a few wavelengths and, therefore, can be used to estimate the aerosol size distribution and the corresponding aerosol scattering-phase function. The aerosol optical thicknesses also can be extrapolated to the near IR. The presence of a forested area that can be used for this purpose can be indicated by the value of the upward radiance in the visible and near IR. A high value of the vegetation index (ratio of the difference of near IR and visible radiances to their sum) indicates dense vegetation [7], while a low value of the radiance detected in the near IR indicates that this vegetation can trap light efficiently by multiple reflections in the canopy, and, therefore, has a low reflectivity in the visible part of the spectrum.

## VII. Atmospheric Correction

The aerosol optical thicknesses derived from the radiances measured from the high-altitude flight over the forest in the off-nadir view are used here to perform atmospheric corrections of the high flight radiances detected over the corn and the pasture. This set of optical thicknesses was chosen since it was derived over a dark land target (except in the near IR). The experiment was conducted in very hazy conditions; therefore, the correction is derived in unfavorable conditions and will enhance any uncertainties in the corrected radiance. The corrected radiance is compared with the measured low flight radiance that serves as the ground truth.

For the correction of the high flight radiances, the same look-up table generated before is used. The surface reflectance $\rho$ is derived from the measured radiance in the high flight $L_H^m$ in a similar way to the determination of the optical thickness: The theoretical function $L_H'(\rho)$ is determined from the look-up table $L_H'(\rho, \tau_a)$ for the optical thickness $\tau_a'$ derived over the forest. The surface reflectance $\rho$ is determined from $L_H'(\rho)$ as the value of $\rho$ that corresponds to the measured radiance $L_H^m$. The corrected radiance $L_H^c$ (that should equal the low flight radiances) is related to the derived surface reflectance $\rho$ by

$$L_H^c = F_D\rho/[\pi(1 - s\rho)]. \tag{6}$$

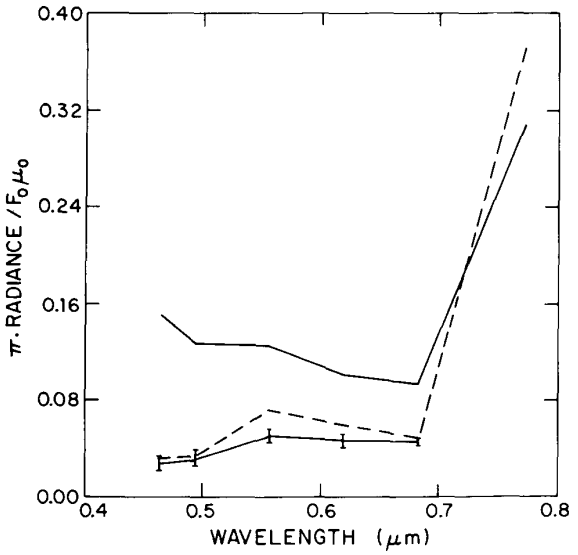


Fig. 12. The upward radiance measured by the OCS over corn ($\theta$ = 25°, $\psi$ = 120°): high flight—at 3800 m (solid line), low flight—at 300 m (dashed line) and the high flight radiances corrected for the atmospheric effect, based on the optical thickness derived from the radiances measured over the forest (Fig. 11(a)-I—I—I).

Note that $L_H^c$ corresponds to the upward radiance at the low flight level rather than the upward radiance at the surface.

The results of the correction are plotted for corn and pasture in Figs. 12 and 13, respectively. The measured high flight radiance and the low flight radiances are also plotted. The atmospheric correction removed most of the atmospheric effect from the data (and sometimes overcorrected the radiances). Due to the strong haziness, the correction reduced the absolute difference between the high and the low flight (normalized) radiances from 0.06–0.12 to 0.0–0.02.

This correction experiment is based on a limited amount of data taken in very hazy conditions, and, therefore, cannot serve as a statistical basis for implementation of a correction algorithm. But it demonstrates the possibility of using dark surface covers (e.g., forest or water) to derive the aerosol characteristics, and to show the ability to perform atmospheric corrections.

The detailed evaluation of the correction and test of the correction procedure is the subject of a future effort. Here (2) can be used to understand the basic features of the correction procedure and the effect of uncertainties in the atmospheric characteristics on the correction. The correction procedure is based on two steps. Derivation of the aerosol optical thickness ($\tau_a$) from radiance $L_1$ detected over a dark surface (e.g., forest in the blue and red parts of the spectrum) of reflectance $\rho_1$

$$L_1 = L_0(\tau_a) + F_D(\tau_a)\, T(\tau_a)\rho_1/\pi \cdot [1 - s(\tau_a)\rho_1] \Rightarrow \tau_a. \tag{7}$$

Since $s$ is a small fraction ($s \leq 0.2$), then for surface reflectance $\rho_1 \leq 0.2$ we can assume, for the purpose of

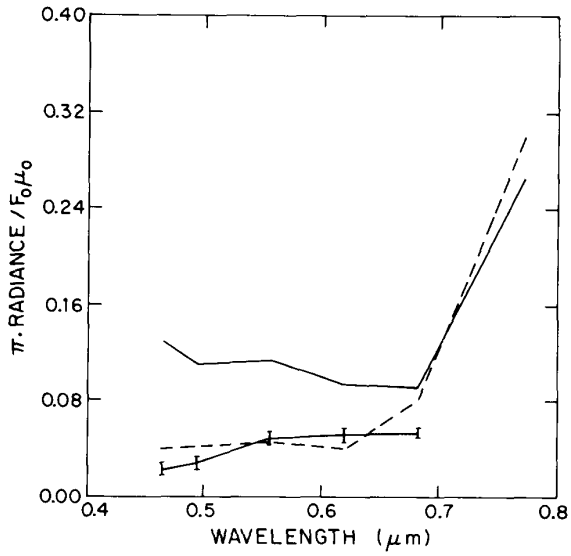


Fig. 13. Same as in Fig. 12 but for pasture ($\theta = 5°$, $\psi = 120°$).

this illustration, that $s\rho_1 \ll 1$

$$L_1 = L_0(\tau_a) + F_D(\tau_a)\, T(\tau_a)\rho_1\pi. \tag{8}$$

The derived value of $\tau_a$ is used for the derivation of the surface reflectance $\rho_2$ from the radiance $L_2$ measured over a different area

$$\rho_2 = \pi(L_2 - L_0)/F_D T \Rightarrow \rho_2 = \rho_1 + \pi(L_2 - L_1)/F_D T. \tag{9}$$

In (9) the path radiance $L_0$, which is the major part of the atmospheric effect for dark surfaces ($\rho \leq 0.1$), was canceled out. Therefore, uncertainties in the derived optical thickness and the other atmospheric optical characteristics will affect the value of $\rho_2$ only through the values of $F_D$ and $T$ and not through $L_0$. This cancellation of $L_0$ decreases the dependence of the error in the derivation of $\rho_2$ on the assumed atmospheric characteristics.

## VIII. Conclusions and Discussion

Aircraft measurements of the upward radiances above and below a haze layer were used to demonstrate the ability of the radiative-transfer model to predict the atmospheric effect on remote sensing of the earth's surface. The wavelength dependence of this effect was measured and simulated by the radiative-transfer model. It was shown that upward radiances measured above a haze layer can be used to derive the aerosol optical thickness in several wavelengths. This derivation is possible for radiance measured above bodies of water and over forested regions (for the visible part of the spectrum). Due to the limited amount of data available in this experiment, and due to sampling differences between the high and the low aircraft flights, the derivation of the optical thickness over forest was performed in only one nadir and one off-nadir case. The derived optical thickness was used for an atmospheric correction of radiances measured over corn and pasture. The difference between the normalized upward radiances in the high and the low flight was reduced from 0.06–0.12 before the correction to 0.0–0.02 after the correction was applied. This correction demonstrates, although it does not prove statistically, that measured optical thicknesses in several wavelengths over dense vegetation (e.g., forest) with high light-trapping ability, can be used to perform atmospheric corrections. The presence of such a surface can be indicated by a high vegetation index (indicating dense vegetation) and a relatively low reflectance in the near IR (indicating the high light trapping). The method can be applied to derive the optical thickness in the visible bands.

## References

[1] Lord Rayleigh (J. W. Strutt), *Phil. Mag.*, vol. 41, pp. 107–274, 1871.
[2] T. N. Carlson and R. S. Caverly, "Radiative characteristics of Saharan dust at solar wavelengths," *J. Geoph. Res.*, vol. 82, pp. 3141–3152, 1977.
[3] J. Prospero, D. L. Savoue, T. N. Carlson, and R. T. Nees, "Monitoring Saharan aerosol transport by means of atmospheric turbidity measurements," Saharan Dust, *Scope*, M. C. Morals, Ed. New York: Wiley, 1979, vol. 14.
[4] Y. J. Kaufman and R. S. Fraser, "Light extinction by aerosols during summer air pollution," *J. Appl. Meteorol.*, vol. 22, pp. 1694–1706, 1983.
[5] —, "The effect of finite field size on classification and atmospheric correction," *Remote Sensing Environ.*, vol. 15, pp. 95–118, 1984.
[6] B. Holben and R. S. Fraser, "Red and near IR sensor response to off-nadir viewing," *Int. J. Rem. Sens.*, vol. 5, pp. 145–160, 1984.
[7] C. J. Tucker, C. Vanpraet, E. Boerwinkel, and A. Gaston, "Satellite remote sensing of total dry matter production in the Senegalese Sahel," *Remote Sensing Environ.*, vol. 13, pp. 461–474, 1983.
[8] Lee and Y. J. Kaufman, "The effect of surface nonlambertianity on remote sensing," *IEEE Trans. Geosci. Remote Sensing*, vol. GE-24, pp. 699–708, no. 5, Sept. 1986.
[9] S. A. W. Gerstl and A. Zardecki, "Discrete-Ordinate finite element method for atmospheric radiative transfer and remote sensing," *Appl. Opt.*, vol. 24, pp. 81–93, 1985.
[10] Y. J. Kaufman, T. W. Brakke, and E. Eloranta, "Field experiment to measure the radiative characteristics of a hazy atmosphere," *J. Atmos. Sci.*, vol. 43, pp. 1135–1151, 1986.
[11] Y. J. Kaufman, "Solution of the equation of radiative transfer for remote sensing over nonuniform surface reflectivity," *J. Geoph. Res.*, vol. 81, pp. 4137–4147, 1982.
[12] S. Chandrasekhar, *Radiative Transfer*. New York: Dover, 1960.
[13] R. S. Fraser and Y. J. Kaufman, "The relative importance of aerosol scattering and absorption in remote sensing," *IEEE Trans. Geosci. Remote Sensing*, vol. GE-23, pp. 625–633, 1985.
[14] J. T. Peterson, E. C. Flowers, G. J. Berri, C. L. Reynolds, and J. H. Rudisil, "Atmospheric turbidity over Central North Carolina," *J. Appl. Meteorol.*, vol. 20, pp. 229–241, 1981.
[15] J. Otterman and R. S. Fraser, "Adjacency effects on imaging by surface reflection and atmospheric scattering: Cross radiance to zenith," *Appl. Opt.*, vol. 18, p. 2852, 1979.
[16] Y. Mekler and Y. J. Kaufman, "The effect of the earth atmosphere on contrast reduction for a nonuniform surface albedo and two-halves field," *J. Geoph. Res.*, vol. 85, pp. 4067–4083, 1980.
[17] Y. J. Kaufman, "Atmospheric effects on remote sensing of surface reflectance," *SPIE*, vol. 475, pp. 20–33, 1984.
[18] J. V. Dave and J. Gazdag, "A modified Fourier transform method for multiple scattering calculations in a plane parallel Mie atmosphere," *Appl. Opt.*, vol. 9, pp. 1457–1466, 1970.
[19] C. E. Junge, *Air Chemistry and Radiochemistry*. New York: Academic, 1963.
[20] J. E. Hansen and L. D. Travis, "Light scattering in planetary atmosphere," *Space Sci. Rev.*, vol. 16, pp. 527–610, 1974.
[21] Z. Ahmed and R. S. Fraser, "An iterative radiative transfer code for ocean-atmosphere system," *J. Atmos. Sci.*, vol. 39, pp. 656–665, 1982.

[22] T. Lee, private communication, 1985.
[23] Y. J. Kaufman, R. S. Fraser, and R. A. Ferrare, "Derivation of the aerosol scattering phase function and absorption from almucantar measurements," Joint IAMAP/IAPSO Ass., Honolulu, Hawaii, 1985.
[24] O. D. Barteneva, "Scattering functions of light in the atmospheric boundary layer," *Izv. Geophys. Ser.*, pp. 1237–1244, 1960.
[25] R. S. Fraser, Y. J. Kaufman, and R. L. Mahoney, "Satellite measurements of aerosol mass and transport," *Atmos. Environ.*, vol. 18, pp. 2577–2584, 1984.
[26] M. D. King, D. M. Byrne, B. M. Herman, and J. A. Reagan, "Aerosol size distribution obtained by inversion of optical depth measurements," *J. Atmos. Sci.*, vol. 35, pp. 2153–2167, 1978.
[27] P. Koepke and H. Quenzel, "Turbidity of the atmosphere determined from satellite calculation of optimum viewing geometry," *J. Geoph. Res.*, vol. 84, pp. 7847–7855, 1979.
[28] K. T. Kriebel, "Reflection properties of vegetated surfaces: Tables of measured spectral biconical reflectance factors," Munchener Universi-tats-Schriften, Meteorologisches Inc., Wissenschaftl. Mitteilung, no. 29, 1977.

**Yoram J. Kaufman** received the B.Sc. and M.Sc. degrees in physics from the Technion-Israel Institute of Technology, Israel, in 1972 and 1974, respectively, and the Ph.D. degree from Tel-Aviv University in 1979.

He is currently working at the Department of Meteorology, University of Maryland, and at the NASA/Goddard Space Flight Center. He conducts both theoretical and experimental research on the atmospheric effect on remote sensing of the Earth's surface, as well as research on the aerosol characteristics from ground-based, aircraft, and satellite observations. He developed a three-dimensional radiative transfer model that is applied to remove the atmospheric effect from satellite images of the Earth. The results of the research are also applied to studies of the transport of regional air pollution aerosol, forest-fire smoke, and Saharan dust.